Metal hydride reactor for dual use: hydrogen storage and cold production

M. Bhouri[a,*], M. Linder[b], I. Bürger[b,*]

[a] Mechanical Engineering, Dalhousie University, B3H 4R2, Halifax, Nova Scotia, Canada

[b] Institute of Engineering Thermodynamics, German Aerospace Center (DLR), D-70569 Stuttgart, Germany

Graphical Abstract

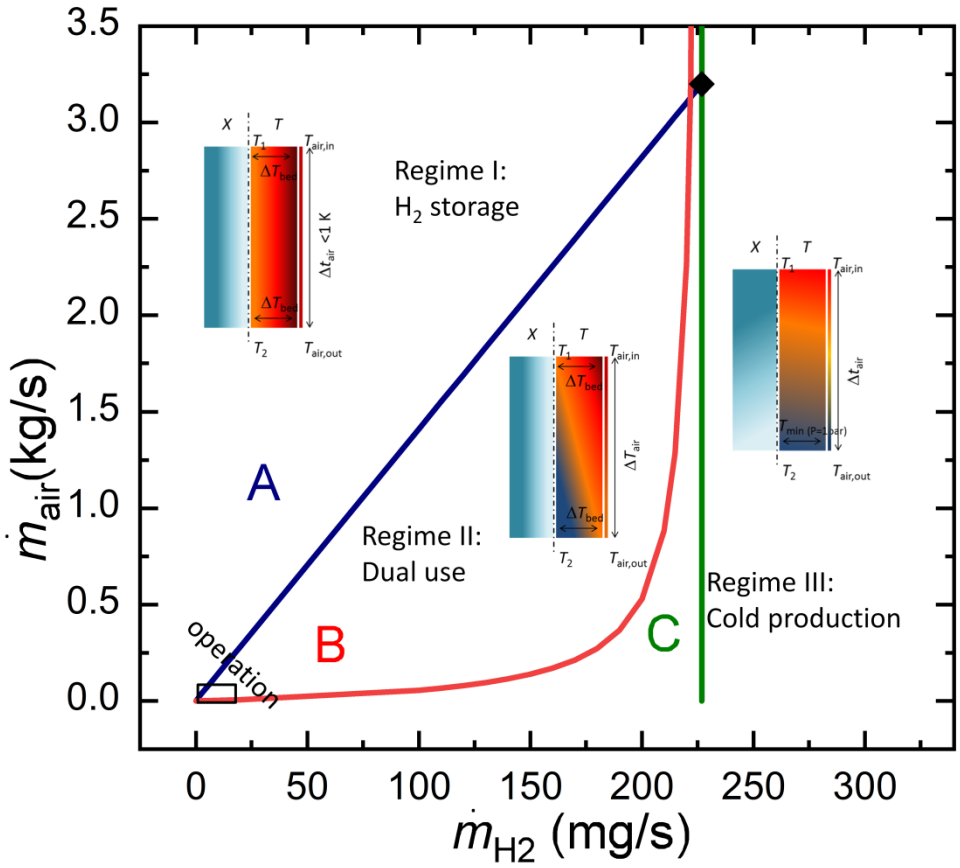

Abstract

In case a metal hydride system is used for gaseous hydrogen storage application, the overall efficiency of the storage system can be significantly improved when the corresponding cooling or heating effect is additionally integrated into the application. In this study, it is analyzed how the efficiency of the gaseous hydrogen storage as well as the temperature level of the cold production can be adjusted using a simple, modular, air-cooled metal hydride reactor. For the study, a Hydralloy C5-graphite composite has been selected as reference material, and as geometry a simple tubular shape has been considered. In the first part of the manuscript, an analytical approach is presented analyzing the three different regimes in which a metal hydride reactor can be operated: to store hydrogen (Regime I), produce cold (Regime III), or to couple both options as "dual use" (Regime II), depending on the mass flow rates of hydrogen and air. In the second part of the manuscript, results of a detailed numerical study are presented and evaluated with respect to the outlet air temperature and the hydrogen utilization factor of the hydride reactor. It is shown that in Regime I, a high utilization factor and in Regime III, low outlet air temperature levels can be reached. Furthermore, in the "dual use" regime, the reactor can produce a cooling effect at different temperature levels and still show a high hydrogen utilization factor. In the last part of the manuscript, the effects of a modular reactor system as well as the operation of the reactor in pressure control mode are discussed to extend the basic description of the problem.

Keywords

Metal hydride
Hydrogen storage
Cold production
Analytical Study
2D simulations

Highlights

- Analytical and numerical studies on hydrogen storage and cold production for metal hydride reactor.
- Three regimes described based on air and hydrogen mass flow rates.
- Evaluation based on outlet air temperature level and hydrogen utilization factor.
- "Dual Use" regime exists with low temperature level and high utilization factor.

*Corresponding authors: Inga Bürger, inga.buerger@dlr.de and Maha Bhouri, maha.bhouri@dal.ca.

1. Introduction

Metal hydrides have been widely studied in the past decades, and it is common sense that they can show excellent properties not only regarding their high volumetric storage capacities, defined pressure and temperature correlations, and high thermal energy densities, but also regarding cycling stability and fast rates of reactions even at low temperatures [1, 2]. Due to these properties, they are suitable for consideration in a wide range of applications that can be basically split into two main categories: First, applications focusing on hydrogen as a gas. Here, next to pure hydrogen storage in metal hydrides [3], also hydrogen compression [4], gas purification [5] or even generation of vacuum with metal hydrides [6] can be mentioned (for a review on all no-storage applications see [7]). Second, there are thermal applications focusing on the heat of reaction when hydrogen is absorbed or released. In this category, heat storage e.g. for pre-heating applications [8], and hydride based air-conditioning systems [9–12] can be enumerated. Obviously, for all these single gaseous or thermal applications, the corresponding coupled effect has to be considered as the hydrogen storage/release and the heat removal/supply occur simultaneously. Thus, for hydrogen storage, a heat management, and for heat storage, a hydrogen supply is required.

Combining different applications and thus using synergies between the linked properties can significantly improve the overall performance of a metal hydride system. This has been already studied for stationary applications, where the heat of reaction is provided /returned to a water based heating system, whenever hydrogen is produced or provided to the fuel cell [13,14]. Another idea for system integration has been presented by Linder et al. [15], where the hydrogen gas for an air conditioning application is not stored in a pressure tank or in a second metal hydride, but the module is integrated in the open hydrogen infrastructure between the high pressure tank and the fuel cell. Furthermore, for vehicle applications, it is common to study hydrogen storage tanks that are integrated into the thermal management of the fuel cell. Thus, the waste heat of the (HT-PEM) fuel cell during driving is used to release hydrogen from the hydride material, increasing then the overall hydrogen storage efficiency [16–18].

Such an increased system integration and combination of effects in one component will get even more important in the future. One example is the need for rather small, lightweight, efficient and safe vehicles required for future mobility in growing cities. A metal hydride tank could combine two existing components: First, it can substitute the 700 bar high pressure hydrogen tank by its low pressure storage solution. Second, as the gaseous hydrogen storage is always accompanied by a thermal effect, it can additionally replace the conventional electric compressor driven air-conditioning system for the passenger cabin. Thus, the enthalpy of reaction for the hydrogen desorption process will not be provided as waste heat by the fuel cell, but it is directly removed from the passenger cabin generating a cooling effect.

Nevertheless, the combination of different functions in one module always implies an increase in system complexity, as different heat and/or mass fluxes have to be controlled at the same time. Furthermore, as the effects are linked, cold is just produced when hydrogen is released and vice versa. Therefore, the goal of the present study is the general analysis of a metal hydride reactor that has the lowest possible system complexity and can still be operated for simultaneous hydrogen release and cold production, which is referred to as "dual use". To this end, any external cooling circuit that is usually implemented for air-conditioning systems is removed, and an air-cooled modular hydride reactor with a simple tubular geometry is considered. A similar geometry has been studied previously as experimental work for stationary hydrogen storage [19], however, without considering the cooling effect. In the present case, it is considered that the air-cooled hydride reactor will directly be connected with the passenger cabin. Thus, in contrast to a fluid cooling circuit where the cooling process has to lower the temperature only by few degrees, in this case the air has to be cooled down from the inlet temperature (e.g. ambient or cabin temperature respectively) to the desired cooling temperature for the cabin.

In this system, the amount of thermal power required to cool air is directly related with the given hydrogen flow rate, as well as the enthalpy of the metal hydride chemical reaction. Thus, the focus of this study is on two aspects: Which hydrogen storage utilization factor, defined as the ratio between the "mass of hydrogen released with relevant flow rates" and the "maximum mass of stored hydrogen that can be discharged" at the corresponding operation conditions [19], can be reached for the reactor – thus how "good" is the reactor as hydrogen storage module. Furthermore, at which temperature level can the cooling effect be provided – thus is there a sensible (cooling) effect in the passenger cabin.

First, for a general view on the problem, the three expected regimes are described, and mathematical descriptions of the regimes are deduced based on the hydrogen and air mass flow rates. Second, a numerical model is set up, validated by the previous experiments and used for a simulation study. The results show the characteristic behavior of the metal hydride reactor for each of the analytically deduced regimes.

2. Model formulation

In this section, first the simplified geometry of the considered module is presented followed by a definition of the operation conditions. Then, analytical expressions using several assumptions are presented, and finally, details of a full numerical model are given.

2.1. Geometry and operation conditions

As discussed earlier, the aim of the present study is to investigate the capability of a modular metal hydride reactor based on a low pressure-low temperature metal hydride, to release hydrogen at a constant mass flow rate, while producing at the same time a sensible cooling effect in the outlet air temperature. As a reference application, a small vehicle is considered where hydrogen is provided to the fuel cell and the cooled outlet air is directed to the passenger cabin. As stated earlier, the fact of

providing both, hydrogen as well as cold, will be referred to as "dual use" of the metal hydride (MeH) reactor in this manuscript.

For this study, a simplified modular reactor configuration consisting of several tubes was considered. Such a design offers flexibility in terms of distribution depending on the space available. The metal hydride is packed inside the central tube with a diameter, d_i; whereas the air flows through the annular duct, with an outer diameter, d_o ,and an insulated outer wall, as shown in Fig. 1.

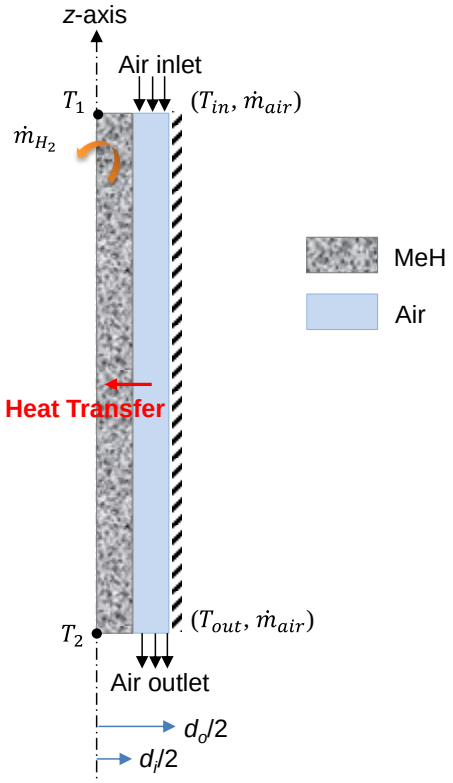

Figure 1. 2D-Axisymmetric geometry of a single MeH - air tube (dimensions are not to scale).

As an assumption, a fuel cell (FC) with an electric power, W_{el} of 2 kW and efficiency, η of 50% was considered. In order to generate the required FC electric power, it was assumed that the H_2 storage system would consist of 10 MeH-air tubes, operating in parallel (200 W_{el}/tube) for one hour (operation time, t_{op} of 60 min).

Similarly to the hydrogen storage system investigated in [19], the Hydralloy C5-graphite composite was used as reference hydrogen storage media, and the diameter of each MeH tube, d_i was set equal to 21 mm. The length of the MeH-air tube is correlated to the electric power of the fuel cell, W_{el}, as well as the operation time required to supply it with hydrogen, t_{op}, as described by the following equations:

$$L_{MeH} = \frac{4}{\rho_{MeH}\,\pi\,d_i^2}\,\frac{\dot{m}_{H_2} t_{op}}{w_{t,max}} \tag{1}$$

where $w_{t,max}$ is the maximum hydrogen storage capacity of the MeH material, and ρ_{MeH} its density.

The mass flow rate of hydrogen to be released, $\dot{m}_{H_2}$ is calculated using the lower heating value of hydrogen (LHV_{H_2} = 242 kJ/mol) as follows [20]:

$$\dot{m}_{H_2} = \frac{\mathrm{W_{el}}}{(1.23 \cdot \eta)} \cdot \frac{M_{H_2}}{2F} \tag{2}$$

where η, M_{H_2}, and F are the FC efficiency, the molar mass of hydrogen, and the Faraday's constant, respectively.

Using the properties of the Hydralloy C5-graphite composite presented in Table 1, and Eqs. (1) and (2), the required hydrogen mass flow rate, $\dot{m}_{H_2}$ and the length of each MeH-air tube, L_{MeH} were found equal to 3.4 mg/s and 77 cm, respectively.

In this study, the backpressure of the fuel cell was set equal to 1 bar. Increasing this pressure will lead to lower hydrogen utilization factors for the given material. However, in case a fuel cell application requires a higher backpressure [21], it is possible to select a different material with a higher equilibrium pressure (see the "Numerical Results and Discussion" section).

Air enters the annular passage at ambient temperature, and constant mass flow rate, $\dot{m}_{air}$ then it is cooled down as heat is transferred to the MeH bed to promote its endothermic desorption reaction, resulting in a temperature gradient between the inlet and outlet.

Recalling that the main goal of this study is to assess the capability of such a system to release hydrogen while providing an air cooling effect inside the vehicle cabin, two variables are crucial for evaluation: First, the outlet air temperature needs to be estimated which is function of the reactor geometry, the MeH and air properties, and the operation conditions in order to evaluate the cooling effect. Next to this outlet temperature, the released amount of hydrogen under constant H_2 mass flow rate desorption condition has to be compared to the maximum stored amount of hydrogen (theoretical best-case conditions), to evaluate how "good" the reactor is as a storage tank. This is equivalent to determining the utilization factor (U.F), defined as the ratio between the "mass of hydrogen released at the desired H_2 mass flow rate" and the "maximum mass of hydrogen that can be discharged" at the corresponding operation conditions.

Two approaches were considered for this problem: First, the described concept was discussed based on a simplified analytical formulation. Thereafter, a two-dimensional mathematical model coupling the kinetics, and heat and mass transfer equations, was developed and solved using the finite element software, COMSOL Multiphysics 5.3. The analytical and numerical results were analyzed for a detailed understanding of the system operation, as well as a possible improvement of its design in order to achieve a higher cooling performance.

Table 1 – Input data used in the modeling of the metal hydride reactor [19, 21, 22]

Parameter	Symbol	Value

Hydralloy C_5-graphite composite (MeH)		
Arrhenius parameter for des (s^{-1})	K_0	6×10^{6}
Activation energy for des (J)	E_A	6.65×10^{-20}
Boltzmann constant (J/K)	k_B	1.38065×10^{-23}
Enthalpy of desorption reaction (J mol^{-1})	ΔH_{des}	28,400
Entropy of desorption reaction (J mol^{-1} K^{-1})	ΔS_{des}	112
Specific heat capacity (J kg^{-1} K^{-1})	$C_{p,bed}$	500
Material density (kg m^{-3})	ρ_{bed}	8,000
Thermal conductivity (W m^{-1} K^{-1})	k_{bed}	7.4
Permeability (m^2)	K	7×10^{-15}
Max. gravimetric H_2 storage capacity	$w_{H,max}$	0.015
Porosity	ε	0.495
Equilibrium Temperature at 1 bar (K)	$T_{eq,1\mathrm{bar}}$	253.15
Hydrogen gas		
molecular weight of gas (g mol^{-1})	M_{H_2}	2.016
Gas constant (J mol^{-1} K^{-1})	R	8.314
Dynamic viscosity (Pa s)	μ_g	$10^{-5}\times9.05\times (T/293)^{0.68}$
Heat capacity (J kg^{-1} K^{-1})	$C_{p,g}$	14,304
Air		
Specific heat capacity of air (J kg^{-1} K^{-1})	$C_{p,air}$	1007
Density of air (kg m^{-3})	ρ_{air}	1.168
Thermal conductivity of air (W m^{-1} K^{-1})	k_{air}	26.03×10^{-3}
Dynamic viscosity of air (Pa s)	μ_{air}	18.48×10^{-6}
Prandtl number	Pr_{air}	0.7141
Inlet air temperature (^{o}C)	$T_{air,in}$	25
Inlet air velocity (m/s)	u_{air}	5 - 120

2.2. Analytical model

As mentioned in the introduction, a metal hydride reactor can be used in different operation modes showing different behavior in e.g. temperature, pressure and conversion. In this manuscript, we describe this behavior referring to the following three operating regimes: Regime I for pure hydrogen storage, Regime III for cold production and Regime II, which is a combination of both ("dual use"). Figure 2 shows schematically the expected temperature (right) and conversion fraction (left) profiles for these three regimes using 2D graphs, to improve the comprehensiveness of the mathematical description in the following. Blue refers to low, red to high temperatures, white to no and turquoise to full conversion.

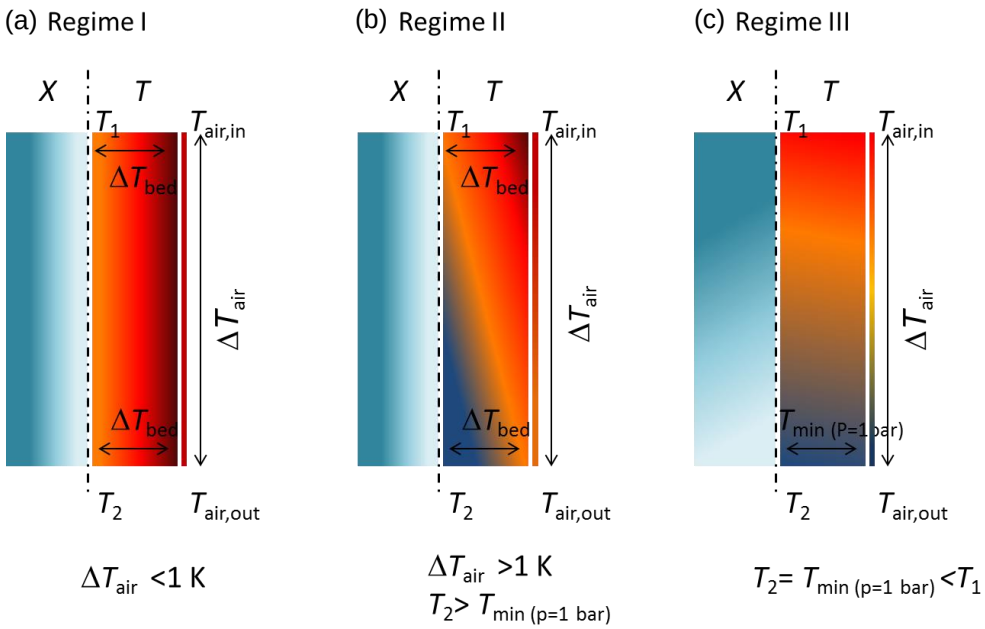

Figure 2. Schematic 2D-plots showing the spatial distributions of temperature (T) and normalized H_2 conversion fraction (X) for regimes (a) I, (b) II, and (c) III.

As in Regime I the focus is on hydrogen storage, it is expected that the temperature gradient in the air region is negligible. Thus, the behavior of the H_2 storage media is characterized by radial gradients, in terms of both, temperature and conversion rate (X) (see Fig. 2 (a)). In contrast, in Regime III (cold production), the reactor reaches at least partially the lowest temperature that is thermodynamically feasible (equilibrium temperature). In this case the reaction is limited by the heat supply of the air at low mass flow rate and as a result, axial gradients dominate the thermal and conversion rate behaviors (see Fig.2 (c)), and the largest temperature gradient between the inlet and outlet of air is expected. Finally, in Regime II (dual use), both effects overlap (see Fig. 2 (b)).

In the following, the analytical expressions describing the behavior in each specific regime will be presented depending on the hydrogen mass flow rate and air mass flow rate. These two parameters can be used to describe the complete system behavior as they are correlated to the heat that must be provided for the H_2 desorption reaction and to the heat that is supplied by the cooling fluid. Overall, using the analytical expressions, a summarizing graph can be drawn that is only dependent on the reactor geometry and material properties.

The main assumption for the mathematical description is based on the fact that the Hydralloy C5-graphite composite can achieve high H_2 desorption rates within few minutes for a pressure range of 1 to 10 bar, as shown in [22]. Thus, the H_2 desorption process is mainly dominated by heat transfer, and the problem considered here can be described according to three governing equations: (i) the temperature gradient between the inlet and outlet of air, (ii) the heat transfer rate that must be supplied to the endothermic H_2 desorption reaction (by the air), and (iii) the temperature gradient over the

hydride bed due to the reaction. Furthermore, the inlet air temperature as well as the equilibrium temperature of the reference material at 1 bar, $T_{eq,1\ bar}$, are restrictions of the problem.

(i) The temperature gradient between the inlet and outlet of air (ΔT_{air}) can be described according to

$$\dot{Q}_{air} = \dot{m}_{air} C_{p,air}\, \Delta T_{air} \tag{3}$$

where $\dot{m}_{air}$ and $C_{p,air}$ are the mass flow rate of air and its specific heat capacity. $\dot{Q}_{air}$ corresponds also to the heat transfer rate from the heat transfer fluid to the hydride material.

(ii) The heat required by the H_2 desorption reaction is defined by the mass flow rate of hydrogen and the desorption reaction enthalpy, and can be expressed as follows:

$$\dot{Q}_{MeH} = \dot{m}_{H_2} \frac{\Delta H_{des}}{M_{H_2}} \tag{4}$$

(iii) The temperature gradient from the surface of the MeH tube to the center of the hydride bed (ΔT_{bed} in Fig. 2) depends on the heat of reaction required during the endothermic desorption process ($\Delta H_{des}/M_{H_2}$), as well as on the heat transfer through the bed (as long as the reactor is in Regime I and II). In case the hydrogen mass flow rate is small compared to the overall amount of stored hydrogen to be released during the desorption process, the mathematical formulation for this gradient is equivalent to the one of one-dimensional heat conduction problem with thermal energy generation due to chemical reaction [23], and the bed temperature gradient can be described as

$$\Delta T_{bed} = \frac{\Delta H_{des}/M_{H_2}}{4 k_{bed} \pi L_{MeH}}\, \dot{m}_{H_2} \tag{5}$$

where ΔH_{des}, M_{H_2}, and k_{bed} are the enthalpy of the desorption reaction, the molecular weight of hydrogen, and the thermal conductivity of the MeH bed, respectively. As this gradient is mainly influenced by the overall mass flow rate of hydrogen, it can be assumed that it is the same for any point along the *z*-axis (see Fig. 2 (a) and (b)). Even though one should note that the absolute values for the temperatures $T_{air,in}$, $T_{air,out}$, T_1 and T_2 can (and will) vary.

Both, Figs. 1 and 2 illustrate the locations of the specified temperatures, which are important to understand the development of this analytical approach, and the following definitions are provided for clarification:

$$\Delta T_{bed} = T_{air,in} - T_1 = T_{air,out} - T_2 \tag{6}$$

where the last equality is only valid in Regime I and II, and

$$\Delta T_{air} = T_{air,in} - T_{air,out} \tag{7}$$

For simplification reasons, the additional temperature gradient caused by the heat transfer from the MeH tube wall to the heat transfer fluid is neglected in the analytical part of this study.

In the following, the spatial distribution of the temperature in the three regimes shown in Fig. 2 is described using Eqs. (3) – (5). Three curves can be deduced that define the limits of the regimes based on $\dot{m}_{H_2}$ and $\dot{m}_{air}$ as shown in Fig. 3 (calculated for the present setup and using the geometric parameters as well as material properties reported in Table 1).

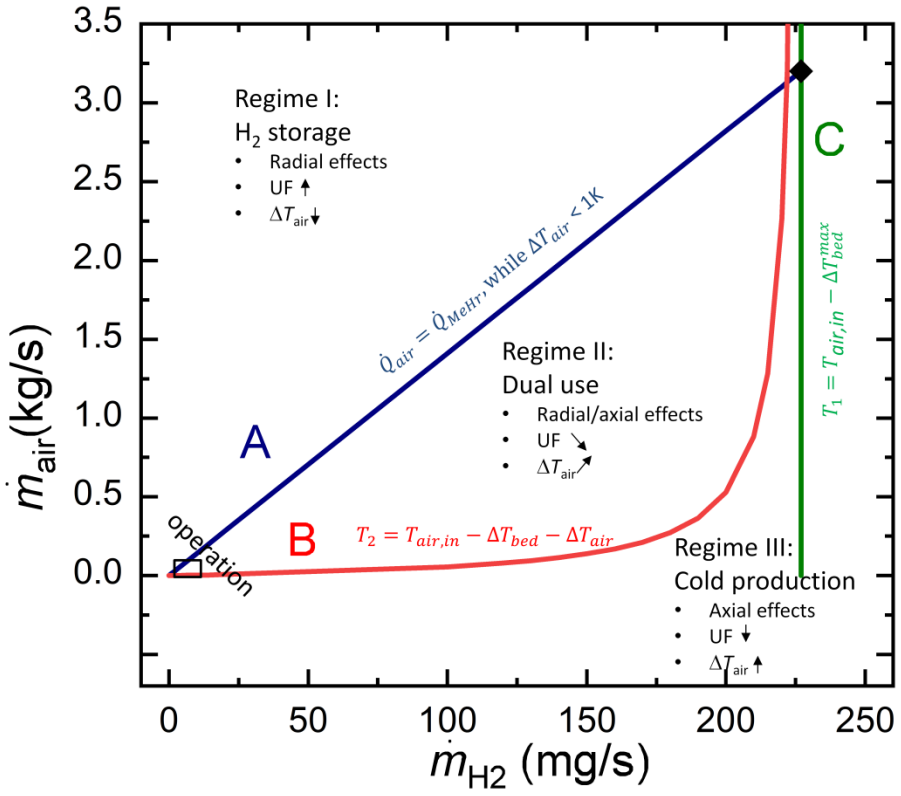

Figure 3. Graphical representation of the different operation regimes of the metal hydride reactor determined analytically.

Regime I*: Hydrogen storage*

As mentioned before, in Regime I, the operation conditions are chosen in a way that the air mass flow rate is very high in comparison to the hydrogen mass flow rate. This implies that the temperature gradient between the air inlet and air outlet is very small – e.g. ΔT_{air} < 1 K. As in this case the conditions for a release of H_2 at constant mass flow rate are optimal, due to the highest possible average temperatures in the reactor, also a high fraction of the stored hydrogen can be released leading to the highest utilization (U.F) factor.

Mathematically, in this regime, the air mass flow rate is sufficient to provide the heat of reaction required to release hydrogen at constant mass flow rate. Thus, the limit of this regime can be calculated based on Eqs. (3) and (4), which leads to air mass flow rates obeying the following inequality:

$$\dot{m}_{air} > \frac{\Delta H_{des}}{M_{H_2}} \frac{1}{C_{p,air}\,\Delta T_{air}^{min}}\,\dot{m}_{H_2} \tag{8}$$

For the graphical representation, $\Delta T_{\mathrm{air}}^{\mathrm{min}}$ = 1 K is used, and the equality of Eq. (8) is denoted as (linear) Curve A in Fig. 3.

Regime II*: Dual use: hydrogen storage and cold production*

In case the MeH reactor should be used not only for hydrogen storage but also for cold production, the reactor performance is evaluated for two criteria: First, a high utilization (U.F) factor for the performance as hydrogen storage module. Second, a low outlet air temperature level in order to be able to actually produce a sensible cooling effect with the amount of cold related to the desorption reaction.

Obviously, it is possible to lower this outlet temperature by lowering the air mass flow rate. However, if the air mass flow rate is decreased too much, the metal hydride reactor is not able to keep up the desired H_2 mass flow rate. Analytically, this point is reached when the temperature T_2, which refers to the lowest temperature in the reactor (see Fig. 1 for its location), reaches the thermodynamically feasible temperature at 1 bar (set as the FC backpressure) for the given material. In this case, T_2 can be determined by substituting Eq. (7) in Eq. (6), thus, when

$$T_2 = T_{air,in} - \Delta T_{bed} - \Delta T_{air} \tag{9}$$

Using Eq. (5) to calculate ΔT_{bed} , and Eq. (3) to calculate ΔT_{air}, and substituting the two obtained expressions in Eq. (9), the second analytical curve restricting Regime II is therefore Curve B (see Fig. 3) with

$$\dot{m}_{air} = \frac{\frac{-\Delta H_{des}/M_{H_2}}{C_{p,air}}\,\dot{m}_{H_2}}{\left(T_2 - T_{air,in}\right) + \frac{\Delta H_{des}/M_{H_2}}{4k_{bed}\pi L_{MeH}}\,\dot{m}_{H_2}} \tag{10}$$

As it was illustrated in the 2D scheme, in Regime II (see Fig. 2 (b)), temperatures do decrease along the *z*-axis, while the radial gradient stays constant (ΔT_{bed} is constant). However, as the effect of the absolute temperature on the reaction is negligible for the given conditions, the front of the reaction is also dominated by a radial effect. This implies that the profiles of the H_2 conversion fractions in Regime I and Regime II are quite similar, and even while additionally producing the desired cooling effect in Regime II, a very high hydrogen utilization factor (U.F) is expected.

Regime III: Cold production

Contrary to Regime I, where the reactor is operated mainly as hydrogen storage module without significant cooling effects, in Regime III, the performance of the reactor is dominated by cooling effects at very low temperatures while the utilization factor (U.F) is very small. Thus, in this regime the metal hydride reactor is used for the desired lowest cooling temperatures. In this case, the

temperature gradient over the bed cannot be calculated by Eq. (5) anymore, as it is mainly limited by the lowest temperature that is thermodynamically feasible.

Analytically, this regime is characterized for values below Curve B on the one side, and it is limited by the maximum hydrogen mass flow rate that can be provided for a minimal time. Thus, if the temperature gradient due to the reaction reaches ΔT_{bed}^{max} even at the position where T_1 is calculated, this means that the temperature T_1 has decreased to the lowest temperature feasible at 1 bar (Equilibrium temperature), and the reaction slows down. This holds true when

$$T_{1,min} = T_{eq,1\ bar} = T_{air,in} - \Delta T_{bed}^{max} \tag{11}$$

This expression is based on the definition of ΔT_{bed} given by Eq. (6). Using Eq. (5), the maximum H_2 flow rate that can be determined for the shortest interval of time, when operating under Regime III is therefore:

$$\dot{m}_{H_2,max} = \frac{\Delta T_{bed}^{max}}{\Delta H_{des}/M_{H_2}} 4 k_{bed} \pi L_{MeH} \tag{12}$$

represented by Curve C in Fig. 3.

If the desired mass flow rate cannot even be provided for a minimal time, the system is on the right-hand side of Curve C. Here, still a cooling effect is observed, however, the utilization factor (U.F) is per definition zero.

An operation in Regime III, thus, resembles more an operation at constant pressure of 1 bar than an operation with constant H_2 mass flow rate.

In order to complete the analytical description, the crossing point of the three curves representative of the characterizing Eqs. (8), (10) and (12) can be given as:

$$\left(\frac{\Delta T_{bed}^{max}}{\Delta H_{des}/M_{H_2}}\ 4 k_{bed} \pi L_{MeH}; \frac{4 k_{bed} \pi L_{MeH}}{C_{p,air}}\ \frac{\Delta T_{bed}^{max}}{\Delta T_{air}^{min}} \right) \tag{13}$$

In Fig. 3, it can be observed that the analytical crossing point matches with Curves A and C, but not exactly Curve B. The reason for this small deviation is the assumption of $\Delta T_{air} < 1$ K in the calculations for the graphical representation. If this value is further reduced, all three lines share exactly the same crossing point.

Obviously, the graph in Fig. 3 gives a very comprehensive summary of the described problem, and it can be a useful tool to study any similar problem, as it can be quickly drawn for any new geometry or any storage media or heat transfer fluid. Looking at all described operating conditions, though, might not always be constructive. For instance, the hydrogen mass flow rate corresponding to Curve C refers to a complete discharge of the reactor in approx. 54 s ($\dot{m}_{H_2}$ = 227 mgs^{-1}), and the compression energy to enable air to flow with a velocity of approx. 8700 m/s which refers to a mass flow rate of 3.2 kg/s, is not realistic for any application.

Therefore, in the following numerical analysis, only a very narrow operation region is considered. This region is marked in a black square in Fig. 3 and corresponds to air mass flow rates of 1.83×10^{-3} to 4.4×10^{-2} kg/s (velocities of 5 to 120 m/s for this geometry), as well as to discharging times of 15 min to 4 hours ($\dot{m}_{H_2}$ of 0.85 to 13.6 mgs^{-1}).

2.3. Numerical model

Following the analytical approach, in this section, a mathematical model describing the physical phenomena taking place in the MeH reactor during the desorption of H_2 is developed and solved in COMSOL Multiphysics 5.3, to gain a better understanding of the different operation regimes. In what follows, the set of equations solved in COMSOL are presented, and the numerical resolution procedure is given in detail.

Mathematical formulation

- MeH bed

As described before, the MeH material considered in this study is a pelletized composite of Hydralloy C5 and graphite [19,22]. During the release of hydrogen, its endothermic desorption reaction can be described by

$$MeH + \Delta_R H \rightarrow Me + \frac{1}{2} H_2 \tag{14}$$

The hydrogen discharging rate is function of the maximum hydrogen storage capacity of the MeH material, $w_{t,max}$, the MeH bed temperature and pressure, T and P, and the equilibrium pressure, $P_{eq,d}$. It can be calculated from the rate equation given by [22]:

$$\frac{\partial w_t}{\partial t} = -K_0 \exp\left(-\frac{E_A}{k_B T}\right)\left(\frac{P - P_{eq,des}}{P_{eq,des}}\right)\cdot\left(w_{t,max} - w_t\right) \tag{15}$$

Two cases are considered for the calculation of the desorption equilibrium pressure, $P_{eq,des}$, either in accordance to the Van't Hoff law with a flat plateau of the pressure-composition isotherms (PCI) curves

$$\frac{P_{eq,des}}{P_0} = exp\left(-\frac{\Delta H_{des}}{RT} - \frac{\Delta S_{des}}{R}\right) \tag{16}$$

or by using the following correlation which offers a high precision of the PCI curves of Hydralloy C5 fit for a temperature range between 0 °C and 100 °C as discussed by Herbrig et al. [22]:

$$\frac{P_{eq,d}}{P_0} = exp\left(a_1 + \frac{a_2}{T} + a_4 w_{t,d}^{\alpha} + a_5 w_{t,d} + a_6 w_{t,d}^2 + a_7 w_{t,d}^3 + a_8 w_{t,d}^4\right) + exp\left(b_1 + b_2 w_{t,d} + b_3 T + b_6 \frac{w_{t,d}}{T}\right) \tag{17}$$

The values of the different constants, a_i and b_i, can be found in [22]. It should also be noted that the weight fraction of the desorbed hydrogen, $w_{t,d}$ is expressed in percentage as $\{100\ (w_{t,max} - w_t)\}$.

Darcy's law is used for the description of the hydrogen gas velocity

$$\vec{v} = -\frac{\mathrm{K}}{\mu_g}\nabla P \tag{18}$$

and the hydrogen mass balance is given by

$$\frac{\partial(\varepsilon\rho_g)}{\partial t} + \nabla\cdot(\rho_g\vec{v}) = -(1-\varepsilon)\dot{m}_R - \dot{m}_{H_2} \tag{19}$$

where K, ε and μ_g are the permeability and the porosity of the MeH bed, and the dynamic viscosity of hydrogen, respectively; ρ_g represents the density of hydrogen given by the ideal gas law ($\rho_g = \frac{PM_{H_2}}{RT}$), and $\dot{m}_R$ refers to the mass change of hydrogen due to the kinetics reaction. It is expressed as

$$\dot{m}_R = \rho_{MeH}\frac{\partial w_{\mathrm{t}}}{\partial t} \tag{20}$$

An additional source term, $\dot{m}_{H_2}$ is defined in the hydrogen mass balance equation to account for the release of hydrogen at a constant mass flow rate as a requirement of the FC operation.

During the endothermic desorption reaction, local thermal equilibrium (LTE) between the hydrogen gas and the MeH bed is assumed. Furthermore, the convective heat transfer of the gas phase is neglected. Accordingly, the energy equation can be written as

$$\left[(1-\varepsilon)C_{p,bed}\rho_{bed} + \varepsilon C_{p,g}\rho_g\right]\frac{\partial T}{\partial t} + \nabla\cdot(-k_{bed}\nabla T) = -(1-\varepsilon)\dot{m}_R\Delta H_R \tag{21}$$

where $C_{p,bed}$ and $C_{p,g}$ are the heat capacities of the hydrogen gas and the MeH bed, k_{bed} is the thermal conductivity of the MeH bed, and ΔH_R is the heat consumed during the desorption reaction, defined as $\Delta H_R = \Delta H_{des}/M_{H_2}$.

- Air region

As a first study of the "dual use" of the MeH reactor for hydrogen storage and air cooling, the thickness of the annular duct where air is flowing, $1/2\,(d_o - d_i)$, was chosen small enough (equal to 4 mm), so that it can be assumed that the air temperature varies only along the length of the MeH tube. The energy equation of the air region is therefore formulated along the axial direction, *z* [24, 25]

$$\rho_{air}C_{p,air}A_{c.s}\frac{\partial T_{air}}{\partial t} + \dot{m}_{air}C_{p,air}\frac{\partial T_{air}}{\partial z} = h_{conv}\pi d_i(T - T_{air}) \tag{22}$$

where ρ_{air} and $C_{p,\mathrm{air}}$ are the density and the heat capacity of air. $A_{c.s}$ refers to the cross sectional-area where air is flowing, defined as $\pi/4\left(d_o^2 - d_i^2\right)$. $\dot{m}_{air}$ denotes the mass flow rate of air, and h_{conv} the heat transfer coefficient between the MeH tube and the air region.

- Initial and boundary conditions

Initially, the MeH material and air are at ambient temperature. The initial pressure of the MeH bed is set equal to 30 bar, which corresponds to the hydrogen supply pressure during the absorption process.

Then, the hydrogen desorption reaction is initiated by removing a constant hydrogen mass flow rate, $\dot{m}_{H_2}$, from the MeH tube in order to feed a FC during a predefined interval of time. This condition is translated into the numerical model by defining $\dot{m}_{H_2}$as a source term in the hydrogen mass balance (see Eq. (19)), and it is still valid as long as the MeH bed pressure does not reach the FC operation backpressure, equal to 1 bar.

Air is forced to flow through the annular duct at constant inlet velocity, u_{air}, and the resulting mass flow rate is calculated as

$$\dot{m}_{air} = \rho_{air}\, u_{air}\, A_{c.s} \tag{23}$$

As the endothermic hydrogen desorption reaction proceeds, the MeH bed temperature decreases, which leads to a heat exchange at the interface between the MeH tube and air flowing at constant mass flow rate, $\dot{m}_{air}$. This can be described by the following equation:

$$\vec{n} \cdot (k_{bed} \nabla T) = h_{conv}\, (T_{air} - T) \tag{24}$$

It should be noted here that the additional energy balance for the MeH tube wall, assumed to be made of stainless steel, was not considered, as the corresponding temperature gradients for this material with high thermal conductivity are rather small.

In the case of this numerical study, the convective heat transfer coefficient, h_{conv} is included and calculated as

$$h_{conv} = \frac{k_{air}\, Nu}{d_h} \tag{25}$$

where k_{air} is the thermal conductivity of air, and d_h is the hydraulic diameter of the annular duct, defined as $d_h = d_o - d_i$.

The outer tube with a diameter, d_o is insulated. With such a condition, and for a fully developed turbulent flow, the Nusselt number, *Nu* is calculated as [26]:

$$Nu = \frac{(\xi_{ann}/8)\, Re_{air}\, Pr_{air}}{k_1 + 12.7\, \sqrt{\xi_{ann}/8}\, \left({Pr_{air}}^{2/3} - 1\right)} \left[1 + \left(\frac{d_h}{L_{MeH}}\right)^{2/3}\right] (0.75\, a^{-0.17}) \tag{26}$$

where a is the diameter ratio, defined as d_i/d_o, Pr_{air} the Prandtl number of air, and Re_{air} its Reynolds number, calculated as

$$Re_{\text{air}} = \frac{4\, \dot{m}_{air}}{\pi (d_o + d_i) \mu_{air}} \tag{27}$$

The friction factor, ξ_{ann} is defined as

$$\xi_{ann} = (1.8\, log_{10}(Re^*) - 1.5)^{-2} \tag{28}$$

The expression of k_1 is given by

$$k_1 = 1.07 + \frac{900}{Re_{air}} - \frac{0.63}{(1 + 10\,Pr_{air})} \quad (29)$$

The properties of the MeH material, hydrogen, and air considered in this study are presented in Table 1. It should be noted that in the case of air, the thermal transport properties were evaluated at an average temperature, $T_{air,Avg} = (T_{air,in} + T_{air,out})/2$, whith $T_{air,in}$ and $T_{air,out}$ are the inlet and outlet temperatures of air, equal to 25 °C and 10 °C. The choice of $T_{air,out}$ was based on the assumption that the MeH reactor would be considered as an efficient cooling device if an outlet air temperature of 10 °C or less is reached. Even though $T_{air,out}$ would vary with the operation conditions, mainly the mass flow rates of hydrogen and air, the same air properties summarized in Table 1 were used for all simulations due to the small variation of the air properties in a temperature range between 0 °C and 25 °C, and therefore, its impact on the calculated heat transfer coefficient given by Eq. (25) was neglected.

Numerical resolution

The set of equations described above was applied to the 2D-axisymmetric geometry presented in Fig. 2 and solved in COMSOL 5.3. A high-quality mesh was generated to provide an accurate mesh-independent solution. To this end, a mapped mesh was used resulting in a total number of elements equal to 1,000. As discussed earlier, depending on the mass flow rates of hydrogen and air, the MeH reactor can be operated as hydrogen storage system, for cold production, or coupling both regimes. To investigate the operation regime, a parametric solver was used to perform a parametric sweep over the two main variables, $\dot{m}_{H_2}$ and u_{air} (which translates to the variation of $\dot{m}_{air}$ as described by Eq. (23)), with a maximum time step of 0.1 s. The simulations were performed over 7200 seconds on a processor Intel Core i7 with 8 GB of RAM, and the computation was completed within a maximum time of 28 minutes.

3. Validation

The mathematical model presented above was first validated for a hydrogen storage system filled with 6 kg of metal hydride-graphite composites (MHCs) [19]. The used MeH material is Hydralloy C5, and the tank is based on 4 layers with 5 tubes each where the MHCs are distributed. Each tube has a diameter of 21 mm and a length of 1.01 m. Four small ventilators were used to blow air, as heat transfer fluid, through a metallic foam structure to ensure an efficient heat exchange during the hydrogen release/storage. The resulting heat transfer coefficient was estimated to be equal to 150 W/(m^2.K). Several desorption/absorption cycles between 4 bar and 30 bar as operating pressures, and 15 °C and 40 °C as operating temperatures, were conducted. Experimental results showed that each layer of the studied system was able to desorb a mass flow rate of hydrogen of 2.7 mg/s. This fulfills the requirement of a fuel cell operating at an electrical power of 160 W_{el} for 100 min.

The same operation and boundary conditions described in [19] were applied to Eqs. (15), (19), and (21), and solved in COMSOL 5.3. Two cases were considered where the equilibrium pressure, $P_{eq,d}$ is described by the Van't Hoff equation (see Eq. (16)), and a realistic PCI correlation (see Eq. (17)). The numerical results showing the distribution of the pressure, bed temperature gradient, and mass of released hydrogen are compared with the corresponding experimental data, as show in Fig. 4. (a) – (c).

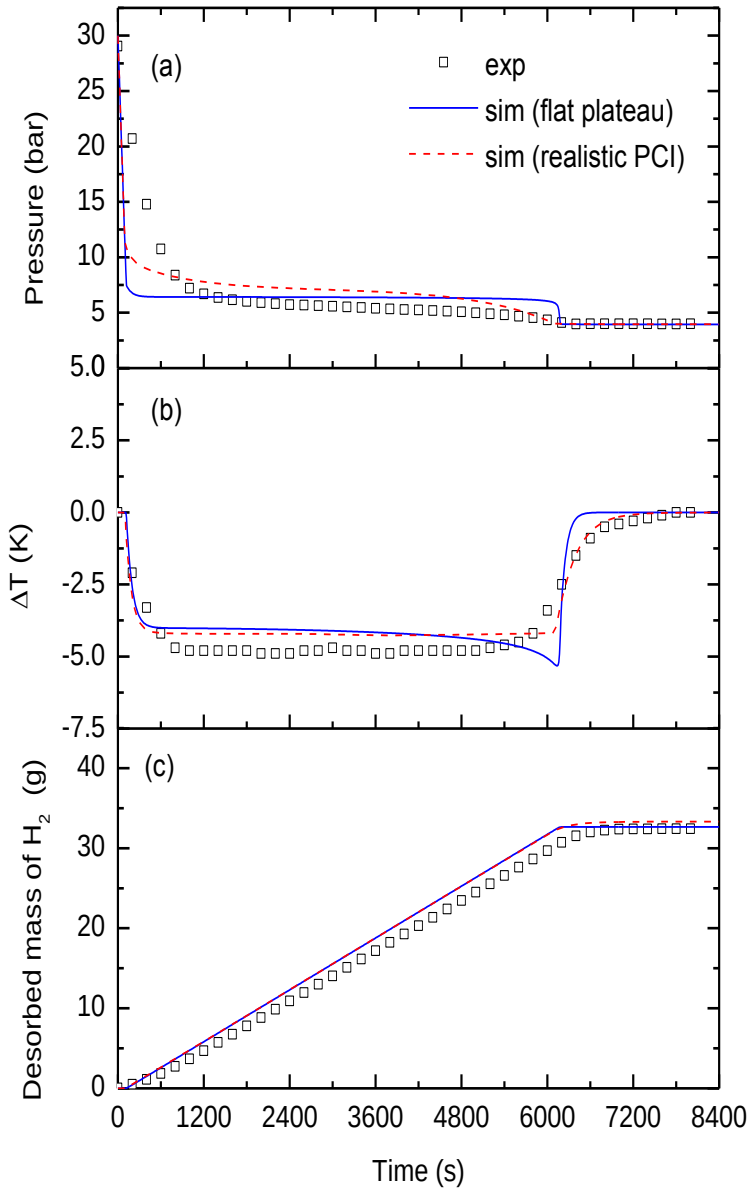

Figure 4. Comparison of the experimental and numerical results for the validation of the numerical model.

From Fig. 4 (a), it can be seen that at the beginning of the desorption process, there is a sharp decrease of the calculated pressure compared to the evolution of the measured value. Such a difference can be due to the removal of the free hydrogen contained in the tubing system during the measurements and was not considered in the simulations. However, this has no effect on the numerical profiles of the bed temperature gradient and the mass of desorbed hydrogen which are in a good agreement with the experimental data, as shown in Fig. 4 (b) and (c).

Thereafter, a pressure plateau is observed which is slightly higher in the case of the simulation results and translates to small differences between the numerical and experimental bed temperature gradients and masses of released hydrogen (see Fig. 4 (b) and (c)). However, the required time for the completion of desorption reaction is still predicted accurately. Indeed, the fuel cell operation backpressure (4 bar) is reached after 100 min, based on both, simulations and measurements (see Fig. 4 (a)), indicating that the maximum amount of hydrogen is removed from the H_2 storage system, as illustrated in Fig. 4 (c).

Furthermore, by comparing the numerical results obtained when the desorption equilibrium pressure, $P_{eq,des}$ is described by the Van't Hoff law (Eq. (16)), and the polynomial function given by Eq. (17), it is obvious that using the Van´t Hoff equation still produces reliable estimates of the H_2 storage system behavior, and can be used to investigate the different operation regimes of the MeH reactor considered in the current study.

4. Numerical Results and Discussion

In this section, the results of the numerical simulations will be presented and discussed in the context of the analytical solution. For clarification, it will be referred to the mass flow rate of hydrogen required by the fuel cell as "desired H_2 mass flow rate", and the one calculated when the desorption reaction is proceeding as "H_2 discharging rate".

4.1. Operation regimes

As described earlier, in order to feed a 2-kW fuel cell (50% of efficiency) during 1 hour, the 10 MeH-air tubes constituting the metal hydride reactor should operate in parallel while providing a constant hydrogen mass flow rate of 3.4 mg/s by each tube. To investigate whether it is possible to keep feeding the fuel cell at the desired H_2 mass flow rate during the entire operation period, a parametric study was conducted where the inlet velocity of air, u_{air} was varied from 5 m/s to 120 m/s, with an incremental step of 5 m/s, for the desired H_2 mass flow rate per MeH-air tube ($\dot{m}_{H_2,des}$ = 3.4 mg/s). Depending on the temporal evolutions of the obtained H_2 discharging rate, and the outlet temperature of air, $T_{air,out}$, presented in Figs. 5 (a) and 6, three operation regimes of the metal hydride reactor were identified. Furthermore, in order to evaluate the hydride reactor as storage module, the utilization factor (U.F) for the different cases is given (see Fig. 5 (b)).

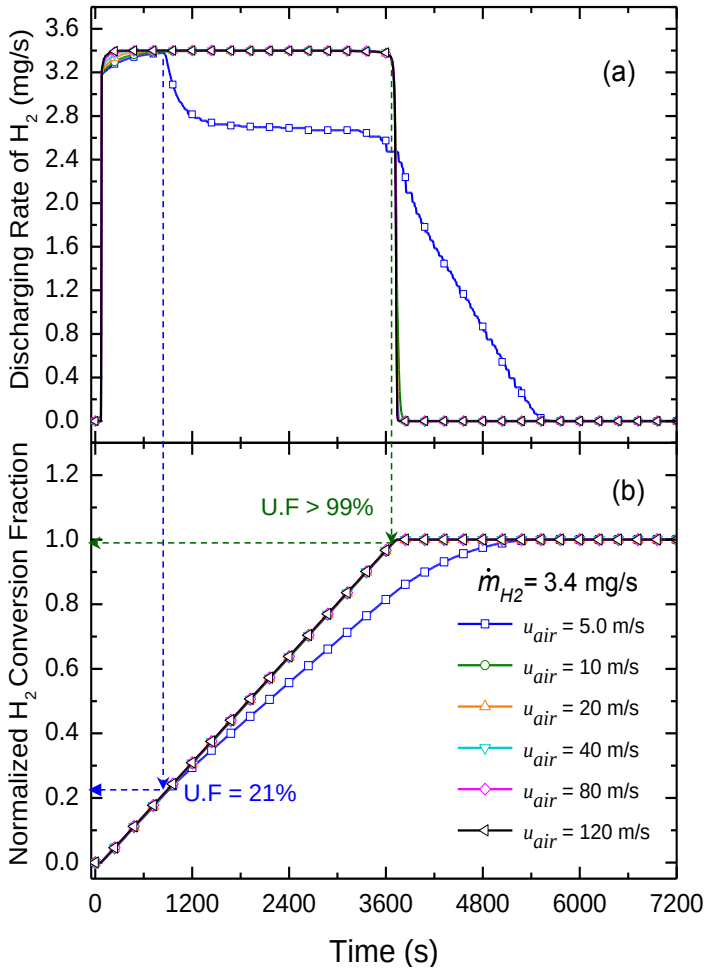

Figure 5. (a) Temporal evolution of the H_2 discharging rate and (b) the corresponding utilization factor, as a function of the air inlet velocity, for a desired H_2 mass flow rate of 3.4 mg/s.

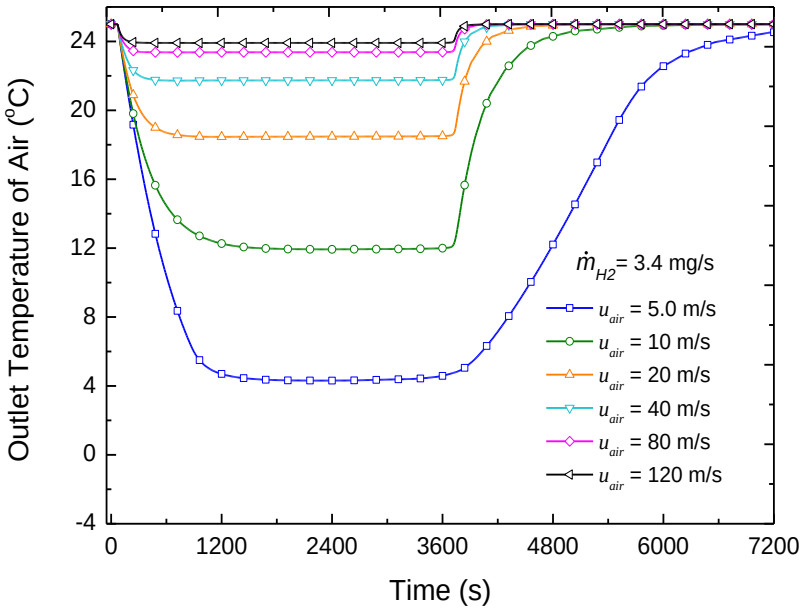

Figure 6. Temporal evolution of the air outlet temperature as a function of the air inlet velocity, for a desired H_2 mass flow rate of 3.4 mg/s.
Regime I*: hydrogen storage*

Operating with an inlet velocity of air, u_{air} equal to 120 m/s corresponds to the case where the metal hydride reactor behaves as a hydrogen storage system. Indeed, it can be seen from Fig. 5 (a), that with such a high air inlet velocity (thus a high mass flow rate of air), it is possible to remove the desired mass flow rate of H_2 (3.4 mg/s) during the operation time of the fuel cell (1 hour); however, the temperature gradient between the inlet and outlet of air does not exceed 1 °C as illustrated in Fig. 6.

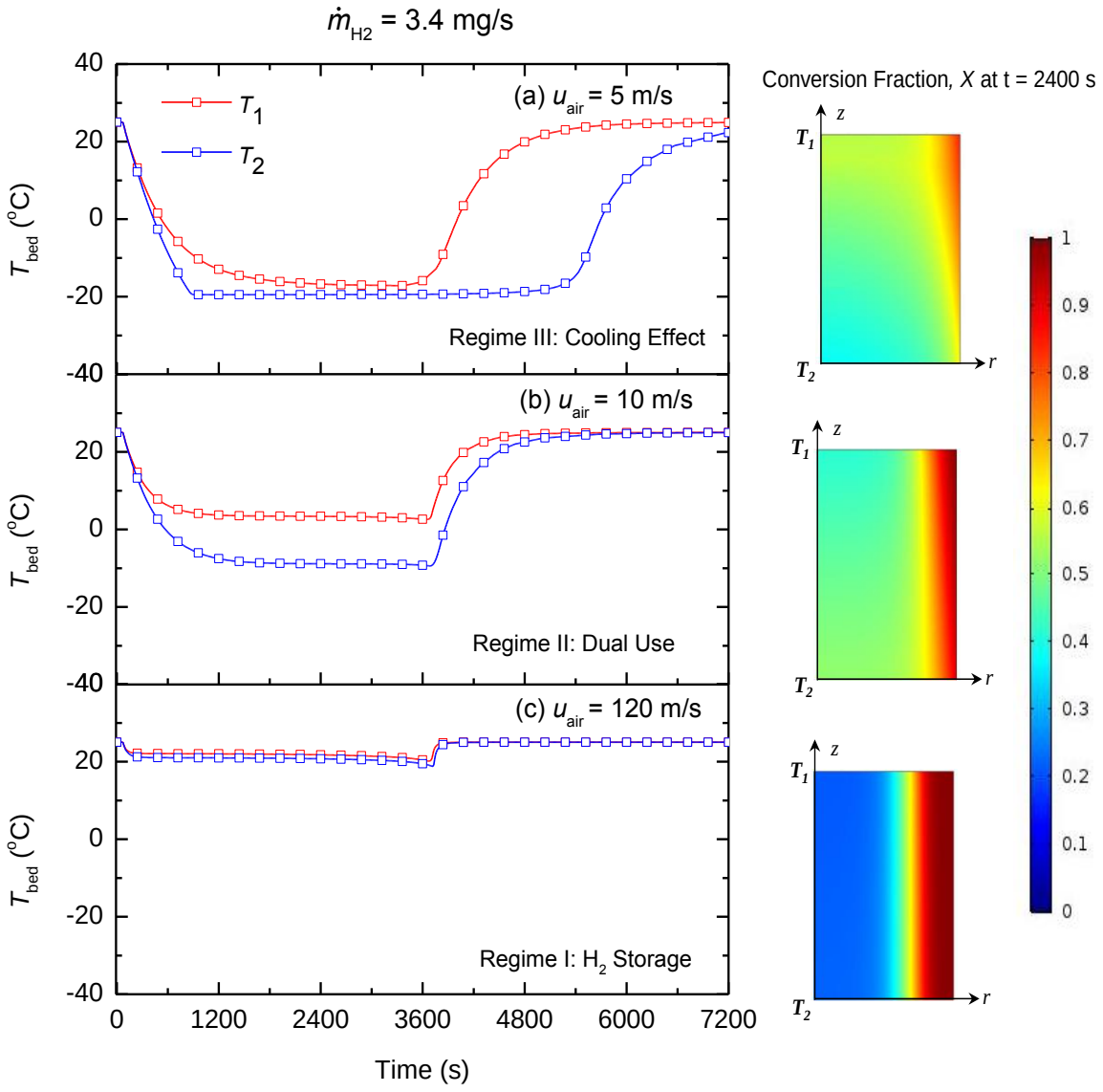

Figure 7. Temporal evolution of the bed temperature at selected locations, and spatial distribution of the normalized H_2 conversion fraction for different operation regimes of the MeH reactor (dimensions of the MeH bed are not to scale)- Desired H_2 mass flow rate set equal to 3.4 mg/s.

Furthermore, by plotting the temporal evolutions of the temperatures T_1 and T_2 located in the center of the bed, and at two different positions along the *z*-axis, when the air inlet velocity is the highest (u_{air} = 120 m/s), it can be seen from Fig. 7 (c), that both, T_1 and T_2, decrease due to the endothermic nature

of the desorption reaction, and then they increase towards the steady-state temperature indicating that the release of H_2 at constant mass flow rate is completed. In addition to this similar trend, only a small difference between T_1 and T_2 is noted when the desorption reaction occurs ($T_1 - T_2 \cong 1$ K). Such a result proves that the temperature profile of the MeH bed changes only in the radial direction, which is in conformity with the description given in the analytical formulation. For a better insight of the described problem, the spatial distribution of the normalized fraction of the released H_2 (X) is also presented in the same figure and shows the expected development of a reaction front in the radial direction. As expected, the final utilization factor reached in these cases is always > 99 % as shown in Fig. 5(b).

Regime II*: dual use: hydrogen storage and cold production*

By lowering the air inlet velocity from 80 m/s to 20 m/s, and further to 10 m/s, it is still possible to desorb hydrogen at constant mass flow rate of 3.4 mg/s, as shown in Fig. 5 (a). At the same time, Fig. 6 shows that for the same air inlet velocities of 10 m/s and 20 m/s, the outlet temperature of air reaches a minimum of 12 °C and 18.5 °C, respectively, in comparison to an inlet temperature of air equal to 25 °C. A plateau of this minimum outlet air temperature is maintained as long as hydrogen is released at constant mass flow rate. Accordingly, the metal hydride reactor provides the desired H_2 mass flow rate while producing an air-cooling effect, which corresponds to the definition of the "dual use" of the metal hydride reactor.

As expected, a cold production on a lower temperature level is achieved for an air inlet velocity of 10 m/s. The resulting temporal evolutions of the temperatures T_1 and T_2 are presented in Fig. 7 (b). As it can be seen, during the dual use of the MeH reactor, a large difference between T_1 and T_2 is noted ($T_1 - T_2 \cong 12$ K), and it is almost kept constant. However, as soon as the release of hydrogen at constant mass flow rate is completed, both, T_1 and T_2 start to increase approximatively at the same time, and their difference is reduced to less than 5 K. Then, it reaches zero once the studied system is at steady-state.

The obtained temperatures profiles suggest that, although different amounts of H_2 are removed from different MeH bed locations (due to the different minimum temperatures reached at locations 1 and 2), the H_2 desorption process is mainly causing radial reaction fronts. Indeed, by plotting the spatial distribution of the normalized fraction of the desorbed H_2, (X) depicted in Fig. 7 (b), a reaction front developing in radial direction can still be observed, similarly to the case of a "hydrogen storage" regime. This can be confirmed by the values of the utilization factor reaching also > 99% for all studied cases, as shown in Fig. 5 (b). Thus, in Regime II, it is not only possible to vary the outlet air temperature to the desired temperature level by varying the air mass flow rate, but also to reach an utilization factor for hydrogen storage as high as the one obtained in Regime I.

Regime III: cold production

Regime III with a dominating cold production effect is obtained for an air inlet velocity of 5 m/s, as illustrated in Figs. 5 (a) and 6. In this case, the MeH reactor is not able to provide the desired H_2 mass flow rate for the whole operation period. Figure 5 (a) shows that a maximum H_2 mass flow rate, slightly smaller than the desired one, is reached at around 850 s, and then it decreases drastically to a value of about 2.7 mg/s where it stabilizes for almost 2750 s and starts decreasing again towards zero. During the stabilization period, a constant outlet air temperature of about 4.5 °C is maintained (see Fig. 6), which is almost three times lower than the one achieved during the "dual use" regime with an air inlet velocity of 10 m/s. As expected, in this case, a utilization factor of about 21% can be reached (see Fig. 5 (b)), and the hydride reactor cannot be considered for hydrogen storage anymore, but only for cold production.

Contrarily to Regimes I (H_2 storage) and II (Dual use) where the differences between T_1 and T_2 were kept constant during the H_2 desorption process at constant mass flow rate, and the temperatures rise was observed after the same interval of time corresponding to the completion of the desorption reaction, Fig. 7 (a) shows different temporal evolutions of T_1 and T_2 when the MeH reactor operates as a cooling device: although a sharp decrease of the temperature is noted at locations 1 and 2, the equilibrium temperature at 1 bar ($T_{eq,1\ bar}$) is reached at location 2, whereas T_1 plotted at the top center of the MeH bed is slightly higher than $T_{eq,1\ bar}$. Thereafter, it takes 3600 s (the operation time required by the fuel cell) to start observing an increase of T_1 towards the steady state temperature of 25 °C, which implies that at that location, the MeH bed is fully discharged. The same trend is observed in the case of T_2 but 1800 s later. Such results suggest that in this "cold production" operation regime, axial gradients of the H_2 discharging rate control the desorption reaction. This is confirmed by the spatial distribution of the normalized fraction of desorbed H_2 (X) plotted in Fig. 7 (a) and showing how the reaction front is developing significantly in the axial direction.

Dependency of Regimes I, II, and III on the FC backpressure

The results presented above for the three identified regimes reflect the behavior of the studied system with a backpressure of 1 bar. In case for the given material the backpressure is increased to a more application relevant value of 5 bar [21], the following trends are expected: For Regime I, there is no effect on the temperature and the utilization factor, while Regimes II and III are significantly influenced. As the equilibrium temperature at 5 bar is 14 °C compared to - 19.5 °C at 1 bar, the maximum allowable temperature difference between the air inlet and the position where T_2 is being calculated is reduced to 11 K. Thus, the system will require higher air flow rates to remain in Regime II (compare Eq. 10), and the hydrogen mass flow rate for which the system reaches Regime III is also reduced (compare Eq. 12). Furthermore, the lowest temperature that can be reached is obviously increased as it is directly related to the equilibrium temperature at the lowest pressure.

In case lower cooling temperatures are required even at higher backpressures, it is an option to select another metal hydride material with a higher equilibrium pressure. For example, in the present case,

Hydralloy C2 could be chosen for a similar application. With this material, at 4.9 bar, the equilibrium temperature is 4 °C [27]. Thus, the overall behavior should be very similar to the presented results with Hydralloy C5 and 1 bar backpressure.

4.2. Modularity

So far, an operation mode with 10 MeH-air tubes feeding the fuel cell in parallel with a H_2 discharging rate of 3.4 mg/s per tube was assumed, and the above results showed that the MeH reactor can be operated in "dual use" regime during one hour when the air inlet velocity is set equal to 20 m/s and 10 m/s, with a higher cooling effect obtained in the latter case.

In this section, the impact of varying the desired mass flow rate of hydrogen, $\dot{m}_{H_2,des}$ on the reactor performance and the cold production is investigated. To this end, a parametric study was conducted where $\dot{m}_{H_2,des}$ was varied from 0.85 mg/s to 13.6 mg/s with an incremental step of 0.85 mg/s while keeping the inlet velocity of air, u_{air} equal to 20 m/s and 10 m/s. The temporal evolutions of the outlet temperature of air and the H_2 discharging rate, as well as the corresponding utilization factor, are presented in Figs. 8 and 9 (a) and (b), and Figs. 10 and 11 (a) and (b), for an inlet air velocity of 20 m/s and 10 m/s, respectively.

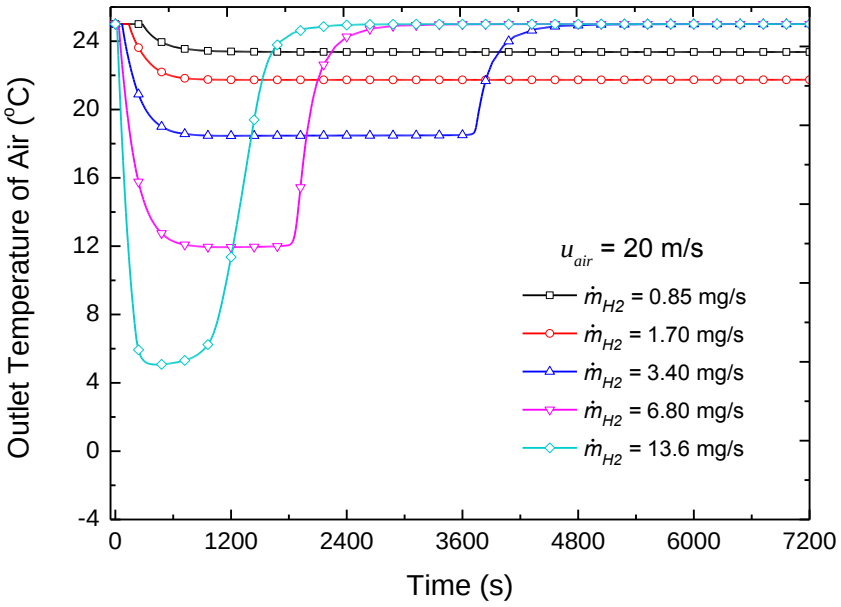

Figure 8. Temporal evolution of the air outlet temperature as a function of the desired H_2 mass flow rate – Air inlet velocity set equal to 20 m/s.

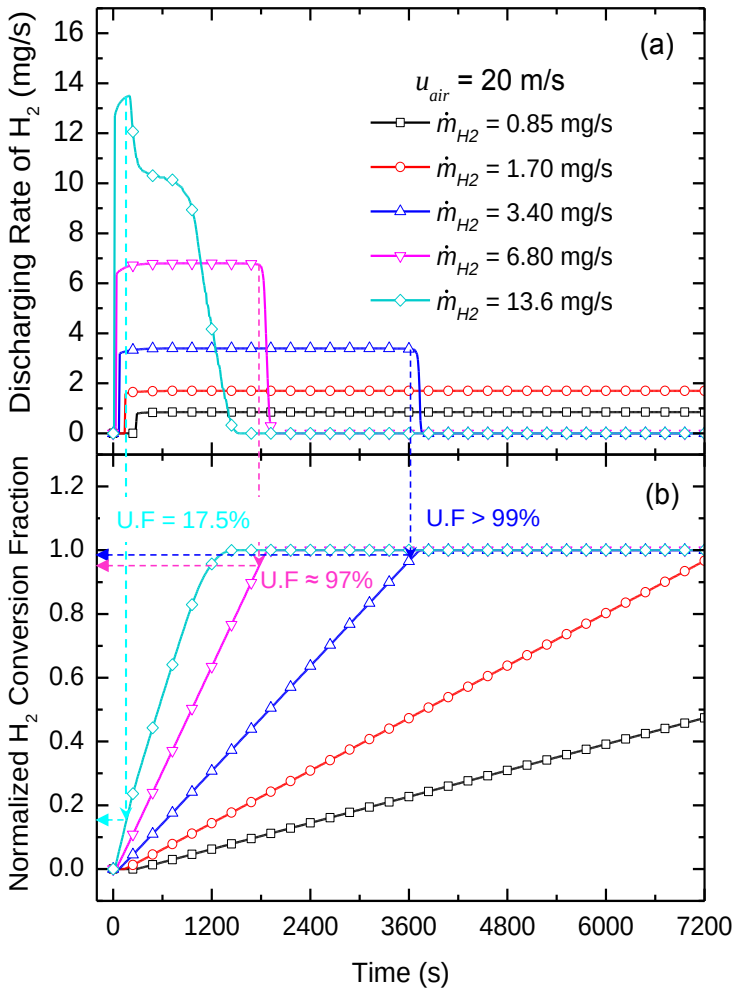

Figure 9. (a) Temporal evolution of the H_2 discharging rate and (b) the corresponding utilization factor, as a function of the desired H_2 mass flow rate – Air inlet velocity set equal to 20 m/s.

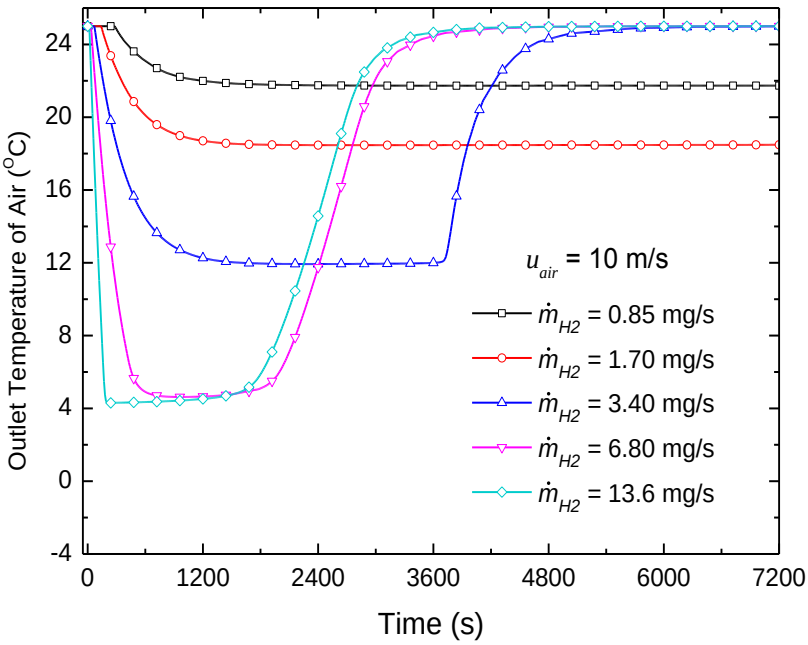

Figure 10. Temporal evolution of the air outlet temperature as a function of the desired H_2 mass flow rate – Air inlet velocity set equal to 10 m/s.

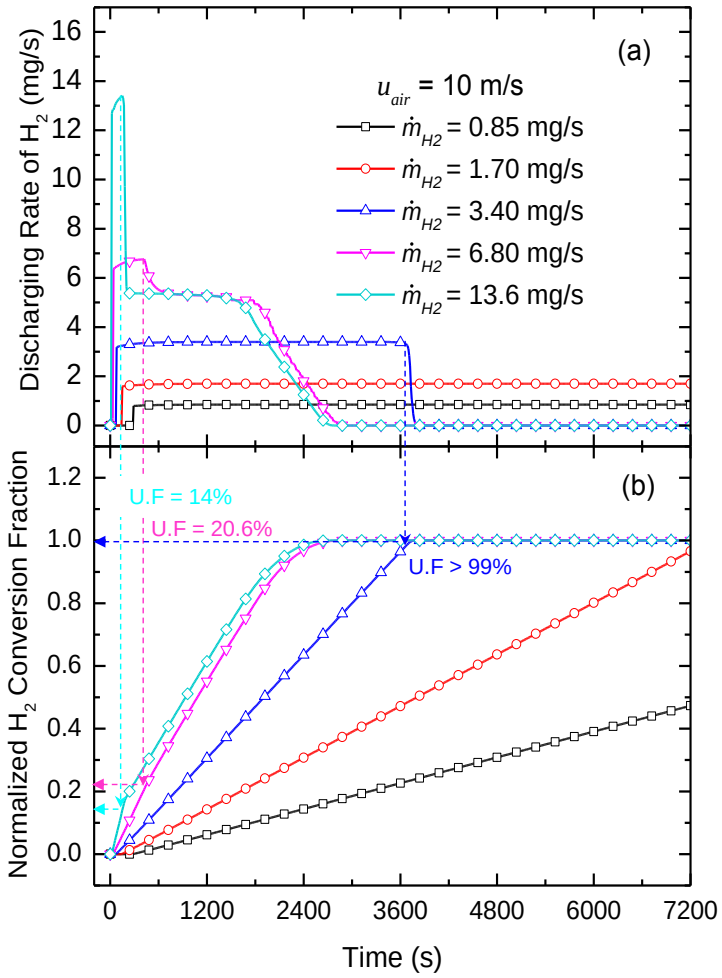

Figure 11. (a) Temporal evolution of the H_2 discharging rate and (b) the corresponding utilization factor, as a function of the desired H_2 mass flow rate – Air inlet velocity set equal to 10 m/s.

Results show that, for the two values of the air inlet velocity, a cooling effect is obtained with a temperature gradient of air varying from 1.5 K as a minimum, to around 21 K as a maximum, depending on the desired mass flow rate of H_2, $\dot{m}_{H_2,des}$. This implies that it is possible to control the outlet air temperature by varying the mass flow rate of H_2; however, as the duration of the reaction varies accordingly, the modularity of the reactor comes into play: By adjusting the number of MeH-air tubes operating at the same time, it is possible to fulfill the requirement of the fuel cell in terms of the total hydrogen mass flow rate, and to keep up the desired total operation time of 1 hour.

For instance, when the air inlet velocity is equal to 20 m/s, the minimum outlet temperature of air can be decreased from 18.5 °C to 12 °C by doubling the H_2 mass flow rate from 3.4 mg/s to 6.8 mg/s (see Fig. 8). However, this also results in half of the stabilization time where a constant minimum outlet temperature and a constant H_2 mass flow rate can be maintained (3600 s when $\dot{m}_{H_2,des}$ is equal to 3.4 mg/s, compared to 1800 s for $\dot{m}_{H_2,des}$ equal to 6.8 mg/s).

Thus, in the first case ($\dot{m}_{H_2,des}$ = 3.4 mg/s), each MeH-air tube can desorb hydrogen at that rate during an operation time of 1 hour. Over that same period, air exits the MeH-air tube at a constant

temperature of 18.5 °C, representing the minimum to reach under the described operation conditions. As it is assumed that the 10 MeH-air tubes operate in parallel during the same interval of time, a total H_2 mass flow rate of 34 mg/s is delivered to the 2-kW fuel cell, resulting in a total amount of discharged hydrogen of 122.4 g.

Now if $\dot{m}_{H_2,des}$ is increased to 6.8 mg/s, in order to keep feeding the 2-kw fuel cell with the total H_2 mass flow rate of 34 mg/s, only 5 MeH-air tubes need to be operating in parallel. At the same time, it is only possible to maintain a constant H_2 discharging rate of 6.8 mg/s per tube and a constant minimum outlet temperature of 12 °C for half an hour (see Figs. 8 and 9 (b)). Thus, for a complete discharge, the two sets of five MeH-air tubes should come into operation in series for half an hour each. This ensures that the total H_2 mass flow rate required by the fuel cell (34 mg/s) is provided for 1 hour while the cooled air exits the MeH-air tube at 12 °C.

When looking at Figs. 8 and 10, it is also worth noting that a same outlet air temperature of 12 °C can be achieved by doubling both, the desired mass flow rate of hydrogen and the air inlet velocity. This can be seen by comparing the minimum reached by $T_{air,out}$ when $\dot{m}_{H_2,des}$ and u_{air} are equal to 3.4 mg/s and 10 m/s, and 6.8 mg/s and 20 m/s, respectively. Again, in order to keep the same value of $T_{air,out}$ during the same operation time, it would be required to adjust the total number of MeH-air tubes operating in parallel, as discussed above.

Figure 8 also shows that for an air inlet velocity of 20 m/s, a further increase of $\dot{m}_{H_2,des}$ to 13.6 mg/s results in a lower temperature of the air exiting the MeH-air tube ($T_{air,out} \cong$ 5 °C), however it is not possible anymore to release hydrogen at constant mass flow rate. In this case, a peak of 13.6 mg/s is first reached, as seen from Fig. 9 (a), then the H_2 discharging rate decreases to a value of 10 mg/s where it stabilizes for a short interval of time, before continuing its decrease towards zero. Here, the utilization factor can be determined to 17.5%, as illustrated in Fig. 9 (b).

The same trend can be observed when the air inlet velocity is set equal to 10 m/s and the desired H_2 mass flow rate is equal to 6.8 mg/s and 13.6 mg/s (see Fig. 11 (a)). Indeed, in both cases, it is not possible to release hydrogen at the desired H_2 mass flow rate, and utilization factors of 14% and 20.6% can be achieved, respectively, as illustrated in Fig. 11 (b); however, the H_2 discharging rate stabilizes at a same value of 5 mg/s for almost the same interval of time. Accordingly, again an outlet air temperature of 4 °C is reached (see Fig. 10), and it is expected that no cold can be produced at a lower temperature by a further increase of the H_2 mass flow rate.

4.3. Pressure control

Following the discussion presented in the analytical formulation section where an operation in the cold production regime (Regime III) would resemble more an operation under pressure control; here, we present the simulation results of a metal hydride reactor desorbing hydrogen at a constant pressure of 1 bar. Three cases were considered where the air inlet velocity was varied from 5 m/s to 10 and 20 m/s,

and the temporal evolutions of the outlet air temperature and the H_2 discharging rate are presented in Fig. 12 (a) and (b).

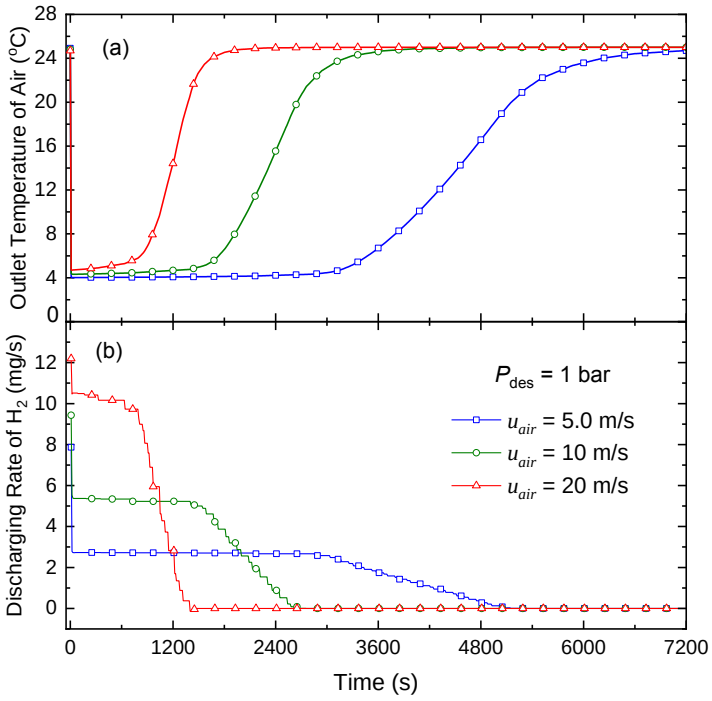

Figure 12. Temporal evolutions of (a) the air outlet temperature and (b) the H_2 discharging rate, as a function of the air inlet velocity, when the MeH reactor is operating under pressure control.

From Fig. 12 (a), it can be seen that a minimum of the outlet air temperature equal to 4 °C is reached when the air inlet velocity is set equal to 5 m/s, and it is kept constant for an interval of time slightly less than one hour. A small rise of that minimum (< 1.5 K) is noticed when the air inlet velocity is increased to 10 m/s and 20 m/s.

However, this results in a shorter period where a temperature plateau can be observed (compare 3300 s in case of u_{air} equal to 5 m/s, to 1740 s and 420 s for u_{air} equal to 10 m/s and 20 m/s, respectively). During these three intervals of time, a desorption process at a constant H_2 discharging rate can be noticed from Fig. 12 (b). Indeed, three plateaus of 2.7 mg/s, 5.3 mg/s and 10 mg/s are obtained for u_{air} equal to 5 m/s, 10 m/s, and 20 m/s, respectively. These findings are similar to those observed when operating under hydrogen mass flow rate control. This can be seen from Fig. 5 for $\dot{m}_{H_2,des}$ = 3.4 mg/s and u_{air} = 5 m/s, from Fig. 11 (a) for $\dot{m}_{H_2,des}$ = 6.8 mg/s and 13.6 mg/s, and u_{air} = 10 m/s, and from Fig. 9 (a) for $\dot{m}_{H_2,des}$ = 13.6 mg/s, and u_{air} = 20 m/s. In addition, for all these cases, the minimum outlet temperature of air was equal to 4 °C, which is the lowest value to reach when the MeH reactor operates in a "cold production" regime.

Thus, pressure-controlled experiments at the lowest desired pressure level give a good estimate on the maximum hydrogen discharging rate that can be removed from the MeH-air tube and can help to define the suitable operation conditions for new reactor modules.

5. Conclusion

In this paper, the possibility of dual use of a metal hydride reactor for hydrogen storage and cold production was investigated based on analytical and numerical studies. A pelletized composite of Hydralloy C5 and graphite was selected as reference material, and a multi-tubular reactor configuration with coaxial tubes was considered, where the metal hydride is filled in the central tube, and air, the heat transfer fluid, flows through the annular duct. The metal hydride reactor was assumed to operate under hydrogen mass flow rate control, so that it would be able to feed a fuel cell at constant hydrogen discharging rate for a duration of 1 hour, as long as the pressure does not reach the fuel cell backpressure, set equal to 1 bar.

It was shown that the metal hydride reactor can be operated in three different regimes that can be described by analytical formulation based on the mass flow rates of hydrogen and air: to store hydrogen (Regime I), produce cold (Regime III), or to couple both options (Regime II).

In order to present a more detailed description of the metal hydride reactor operation in the three identified regimes, a series of simulations was conducted in COMSOL Multiphysics 5.3, and the numerical results were in agreement with the analytical findings.

Overall, it was shown that when a constant hydrogen mass flow rate is desired for the specific operation time required by the fuel cell, this can be ensured when a very high air mass flow rate is used. In this case, the metal hydride reactor behaves as a hydrogen storage system, resulting in the highest utilization factor. For a very low air mass flow rate, only cold can be produced, and it would not be possible to keep discharging hydrogen at the desired rate, thus only low utilization factors can be reached. Finally, for a certain range of the air mass flow rate in between, both hydrogen storage with high utilization factors, and air-cooling effect can be ensured; however different temperature levels are reached by the exiting cold air. Furthermore, it was shown that depending on the operation regime, metal hydride temperature gradients and reaction front gradients would develop in radial direction for Regimes I and II, and in axial direction in Regime III.

Simulation results also showed that, for a given mass flow rate of air, it is possible to reach lower temperature levels of the cold air exiting the metal hydride reactor by increasing the mass flow rate of hydrogen to be released. In this case, the number of MeH-air tubes operating at the same time should be adjusted to still feed the fuel cell at the required hydrogen mass flow rate for the whole operation period.

It was also noticed that there exists a minimum to reach for the outlet air temperature, which is directly correlated to the thermodynamically feasible temperature of the metal hydride bed (equilibrium

temperature at 1 bar). Thus, a hydrogen discharging process at constant pressure can provide two main pieces of information: the maximum hydrogen discharging rate to remove, and the minimum outlet air temperature to reach. As such an experiment represents a good estimate for suitable operation conditions of the metal hydride reactor, it is suggested to perform it first as experimental characterization.

To conclude, it should be emphasized that even though the analytical study was applied to a specific metal hydride, and specific reactor geometry, it can be generalized to optimize the operation conditions for "dual use" of any metal hydride system, since it is only based on the geometric properties of the reactor, the properties of the reactive material, and the mass flow rates of hydrogen and heat transfer fluid.

Acknowledgements

M.B. would like to thank the German Academic Exchange Service (DAAD) for the DLR-DAAD Research Fellowship.

References

[1] Schlapbach L, editor. Hydrogen in Intermetallic Compounds I. Berlin, Germany: Springer; 1988.

[2] Schlapbach L, editor. Hydrogen in Intermetallic Compounds II. Berlin, Germany: Springer; 1988.

[3] Sakintuna B, Lamari-Darkrim F, Hirscher M, Lamaridarkrim F. Metal hydride materials for solid hydrogen storage: A review. Int J Hydrogen Energy 2007;32:1121–40. doi:10.1016/j.ijhydene.2006.11.022.

[4] Lototskyy MV, Yartys V a., Pollet BG, Bowman RC. Metal hydride hydrogen compressors: A review. Int J Hydrogen Energy 2014;39:5818–51. doi:10.1016/j.ijhydene.2014.01.158.

[5] Saitou T, Sugiyama K. Hydrogen purification with metal hydride sintered pellets using pressure swing adsorption method. J Alloys Compd 1995;231:865–70. doi:10.1016/0925-8388(95)01774-7.

[6] Prina M, Kulleck JG, Bowman RC. Assessment of Zr–V–Fe getter alloy for gas-gap heat switches. J Alloys Compd 2002;330-332:886–91.

[7] Bhuiya MMH, Kumar A, Kim KJ. Metal hydrides in engineering systems, processes, and devices: A review of non-storage applications. Int J Hydrogen Energy 2015;40:2231–47. doi:10.1016/j.ijhydene.2014.12.009.

[8] Dieterich M, Bürger I, Linder M. Open and closed metal hydride system for high thermal power applications: Preheating vehicle components. Int J Hydrogen Energy 2017;42. doi:10.1016/j.ijhydene.2017.03.024.

[9] Muthukumar P, Groll M. Metal hydride based heating and cooling systems: A review. Int J Hydrogen Energy 2010;35:3817–31. doi:10.1016/j.ijhydene.2010.01.115.

[10] Weckerle C, Buerger I, Linder M. Novel reactor design for metal hydride cooling systems. Int J Hydrogen Energy 2017:1–12. doi:10.1016/j.ijhydene.2017.01.066.

[11] Ni J, Liu H. Experimental research on refrigeration characteristics of a metal hydride heat pump in auto air-conditioning. Int J Hydrogen Energy 2007;32:2567–72. doi:10.1016/j.ijhydene.2006.09.038.

[12] Linder M, Mertz R, Laurien E. Experimental results of a compact thermally driven cooling system based on metal hydrides. Int J Hydrogen Energy 2010;35:7623–32. doi:10.1016/j.ijhydene.2010.04.184.

[13] Nakano A, Ito H, Maeda T, Munakata T, Motyka T, Corgnale C, et al. Study on a metal hydride tank to support energy storage for renewable energy. J Alloys Compd 2013;580:S418–22. doi:10.1016/j.jallcom.2013.03.152.

[14] Maeda T, Nakano A, Ito H, Tange M, Kawakami Y, Kato A, et al. The Development of the Totalized Hydrogen Energy Utilization System for Commercial Buildings. J Int Counc Electr Eng 2014;1:194–9. doi:10.5370/JICEE.2011.1.2.194.

[15] Linder M, Kulenovic R. An energy-efficient air-conditioning system for hydrogen driven cars. Int J Hydrogen Energy 2011;36:3215–21. doi:10.1016/j.ijhydene.2010.11.101.

[16] Urbanczyk R, Peil S, Bathen D, Heßke C, Burfeind J, Hauschild K, et al. HT-PEM Fuel Cell System with Integrated Complex Metal Hydride Storage Tank. Fuel Cells 2011;11:911–20. doi:10.1002/fuce.201100012.

[17] Weiß-Ungethüm J, Bürger I, Schmidt N, Linder M, Kallo J. Experimental investigation of a liquid cooled high temperature proton exchange membrane (HT-PEM) fuel cell coupled to a sodium-alanate tank. Int J Hydrogen Energy 2014;39:5931–41.

[18] Adametz P, Müller K, Arlt W. Energetic evaluation of hydrogen storage in metal hydrides. Int J Energy Res 2016;40:1820–31. doi:10.1002/er.

[19] Bürger I, Dieterich M, Pohlmann C, Röntzsch L, Linder M. Standardized hydrogen storage module with high utilization factor based on metal hydride-graphite composites. J Power Sources 2017;342:970–9. doi:10.1016/j.jpowsour.2016.12.108.

[20] Larminie J, Andrew Dicks. Fuel Cell Systems Explained. John Wiley & Sons; 2003. doi:10.1002/9781118878330.

[21] U.S. DRIVE (Driving Research and Innovation for Vehicle efficiency and Energy sustainability). Target Explanation Document: Onboard Hydrogen Storage for Light-Duty Fuel Cell Vehicles. 2017. doi:https://www.energy.gov/sites/prod/files/2017/05/f34/fcto_targets_onboard_hydro_storage_explanation.pdf.

[22] Herbrig K, Röntzsch L, Pohlmann C, Weißgärber T, Kieback B. Hydrogen storage systems based on hydride–graphite composites: computer simulation and experimental validation. Int J Hydrogen Energy 2013:1–11. doi:10.1016/j.ijhydene.2013.03.104.

[23] Incropera FP, DeWitt DP, Bergman TL, Lavine AS. Fundamentals of Heat and Mass Transfer. 6th ed. John Wiley & Sons; 2006.

[24] Massoud Kaviany. Essentials of Heat Transfer: Principles, Materials, and Applications. Cambridge University Press; 2011.

[25] Chung C a. A, Ho C-J. Thermal-fluid behavior of the hydriding and dehydriding processes in a metal hydride hydrogen storage canister. Int J Hydrogen Energy 2009;34:4351–64. doi:10.1016/j.ijhydene.2009.03.028.

[26] VDI Heat Atlas. 2nd ed. 20. Springer; 2010.

[27] Skripnyuk V, Ron M. Hydrogen desorption kinetics in intermetallic compounds C2, C5 and C5 with Laves phase structure. Int J Hydrogen Energy 2003;28:303–9. doi:10.1016/S0360-3199(02)00081-2.

Nomenclature

Abbreviations

FC	Fuel Cell
LHV	Lower Heating Value
LTE	Local Thermal Equilibrium
MeH	Metal Hydride
U.F	Utilization Factor

Variables

A	Surface area (m^2)
C_p	Specific heat capacity ($J/kg^{-1} K^{-1}$)
d	Diameter (m)
E_A	Activation energy (J)
F	Faraday's constant ($C\ mol^{-1}$)
h	Heat transfer coefficient ($W\ m^{-2} K^{-1}$)
k	Thermal conductivity ($W\ m^{-1} K^{-1}$)
k_B	Boltzmann constant ($J\ K^{-1}$)
K	Permeability (m^2)
K_0	Arrhenius parameter (s^{-1})
L	Length (m)
M	Molecular weight ($kg\ mol^{-1}$)
$\dot{m}$	Mass flow rate ($mg\ s^{-1}$) or ($kg\ s^{-1}$)
$\vec{n}$	Normal vector
Nu	Nusselt number
P	Pressure (Pa)
P_{eq}	Equilibrium pressure (Pa)
P_0	Atmospheric pressure (Pa)
Pr	Prandtl number
$\dot{Q}$	Heat transfer rate (W)
R	Universal gas constant ($J\ mol^{-1} K^{-1}$)
Re	Reynolds number
t	Time (s)
T	Temperature (°C)
u	Velocity (m/s)
$\vec{v}$	Velocity (m/s)
w_t	Gravimetric H_2 storage capacity (-)
W	Power (W)
X	Normalized fraction of desorbed H_2 (-)

Greek Letter

ΔH	Enthalpy of reaction (kJ mol^{-1})
ΔS	Entropy of reaction (kJ K^{-1} mol^{-1})
ε	Porosity (-)
η	Efficiency (%)
μ	Dynamic viscosity (Pa s)
ξ_{ann}	Friction factor
ρ	Mass density (kg m^{-3})

Subscripts

air	Associated with air
Avg	Average
bed	Associated with metal hydride bed
conv	Convection
c.s	Cross section
des	Desorption
el	Electric
eq	Equilibrium
g	Gas
h	Hydraulic
H_2	Associated with hydrogen gas
i	Inner
in	Inlet
max	Maximum
MeH	Associated with metal hydride
o	Outer
op	Operation
out	Outlet
R	Reaction

Superscripts

min	Minimum
max	Maximum